8350 *Biochemistry* **2010,** *49,* 8350–8358
DOI: 10.1021/bi1005283

BIOCHEMISTRY
including biophysical chemistry & molecular biology
Article

Novel Benzimidazole Inhibitors Bind to a Unique Site in the Kinesin Spindle Protein Motor Domain[†]

Payal R. Sheth,*[,‡,△] Gerald W. Shipps Jr.,[§,△] Wolfgang Seghezzi,[⊥] Catherine K. Smith,[‡] Cheng-Chi Chuang,[‡] David Sanden,[⊥] Andrea D. Basso,[#] Lev Vilenchik,[‡] Kimberly Gray,[#] D. Allen Annis,[▽] Elliott Nickbarg,[∥] Yao Ma,[§] Brian Lahue,[§] Ronald Herbst,[◇] and Hung V. Le[‡]

[‡]*Protein Science Department,* [§]*Lead Discovery Chemistry Department, and* [∥]*Biology Department, Merck Research Laboratories, 320 Bent Street, Cambridge, Massachusetts 02141,* [⊥]*Tumor Biology Department, Merck Research Laboratories, 901 California Avenue, Palo Alto, California 94304, and* [#]*Tumor Biology Department, Merck Research Laboratories, 3000 Galloping Hill Road, Kenilworth, New Jersey 07033.* [△]*Both authors contributed equally to this publication.* [▽]*Present address: Aileron Therapeutics, Inc., 840 Memorial Drive, Cambridge, MA 02139.* [◇]*Present address: MedImmune, One MedImmune Way, Gaithersburg, MD 20878.*

Received April 8, 2010; Revised Manuscript Received August 16, 2010

ABSTRACT: Affinity selection−mass spectrometry (AS-MS) screening of kinesin spindle protein (KSP) followed by enzyme inhibition studies and temperature-dependent circular dichroism (TdCD) characterization was utilized to identify a series of benzimidazole compounds. This series also binds in the presence of Ispinesib, a known anticancer KSP inhibitor in phase I/II clinical trials for breast cancer. TdCD and AS-MS analyses support simultaneous binding implying existence of a novel non-Ispinesib binding pocket within KSP. Additional TdCD analyses demonstrate direct binding of these compounds to Ispinesib-resistant mutants (D130V, A133D, and A133D + D130V double mutant), further strengthening the hypothesis that the compounds bind to a distinct binding pocket. Also importantly, binding to this pocket causes uncompetitive inhibition of KSP ATPase activity. The uncompetitive inhibition with respect to ATP is also confirmed by the requirement of nucleotide for binding of the compounds. After preliminary affinity optimization, the benzimidazole series exhibited distinctive antimitotic activity as evidenced by blockade of bipolar spindle formation and appearance of monoasters. Cancer cell growth inhibition was also demonstrated either as a single agent or in combination with Ispinesib. The combination was additive as predicted by the binding studies using TdCD and AS-MS analyses. The available data support the existence of a KSP inhibitory site hitherto unknown in the literature. The data also suggest that targeting this novel site could be a productive strategy for eluding Ispinesib-resistant tumors. Finally, AS-MS and TdCD techniques are general in scope and may enable screening other targets in the presence of known drugs, clinical candidates, or tool compounds that bind to the protein of interest in an effort to identify potency-enhancing small molecules that increase efficacy and impede resistance in combination therapy.

Kinesin spindle protein (KSP[1] or Eg5), a member of the kinesin-5 family, is required for separation of duplicated spindle poles in prometaphase and thus is critical for the formation of a bipolar mitotic spindle (*1*). Members of the kinesin-5 family share a conserved N-terminal catalytic motor domain followed by a short (12−15 amino acids) linker leading to a coiled stalk. Functionally, KSP is a bipolar heterotetramer composed of two polypeptides that dimerize first to form a parallel coiled coil; then the two dimers tetramerize into an antiparallel coiled coil exhibiting two motor domains each at the distal ends. The two pairs of motor domains bridge adjacent microtubules and use energy derived from ATP hydrolysis to slide the two strands relative to each other (*2*, *3*).

KSP is required at the early stage of mitosis and has received considerable attention as a drug target (*1*, *4*, *5*). Inhibition of KSP motor function results in mitotic arrest that is characterized by a misformed mitotic spindle (*6*). In cancer cells, inhibitors of KSP may therefore induce cell cycle arrest and lead to cancer cell death (*7*, *8*). Toward this end, numerous small molecule KSP inhibitors have been reported; among them are dihydropyrimidinethione **1** (monastrol) (*8*) and quinazolinones from Cytokinetics (Ispinesib, Figure 1a) (*7*). Several KSP series have been advanced to preclinical or clinical studies, and ongoing recent publications from multiple companies highlight the high level of interest in KSP as an anticancer biological target (*9*−*14*). All of the disclosed series that have advanced into preclinical development for KSP have been shown to bind at the monastrol binding site, including Ispinesib (*5*, *15*).

[†]The work was funded by Schering-Plough Corp. (now a part of Merck & Co., Inc.).

*To whom the correspondence may be addressed. E-mail: payal.sheth@spcorp.com. Phone: 617-499-3643. Fax: 617-499-3814.

[1]Abbreviations: KSP (Eg5), kinesin spindle protein; MT, microtubules; SDS, sodium dodecyl sulfate; ATP, adenosine 5′-triphosphate; ADP, adenosine 5′-diphosphate; CD, circular dichroism; TdCD, temperature-dependent circular dichroism; DMSO, dimethyl sulfoxide; HEPES, *N*-(2-hydroxyethyl)piperazine-*N*′-2-ethanesulfonic acid; SEC, size-exclusion chromatography; RPC, reversed-phase chromatography; AS-MS, affinity selection−mass spectrometry; ALIS, automated ligand identification system; PIPES, piperazine-1,4-bis(2-ethanesulfonic acid); DTT, dithiothreitol; ESI-MS, electrospray ionization−mass spectrometry; LC-MS, liquid chromatography−mass spectroscopy; TCEP, tris(2-carboxyethyl)phosphine hydrochloride; Asp (D), aspartic acid; Ala (A), alanine; rms, root mean square; WT, wild type.

 Published on Web 08/18/2010

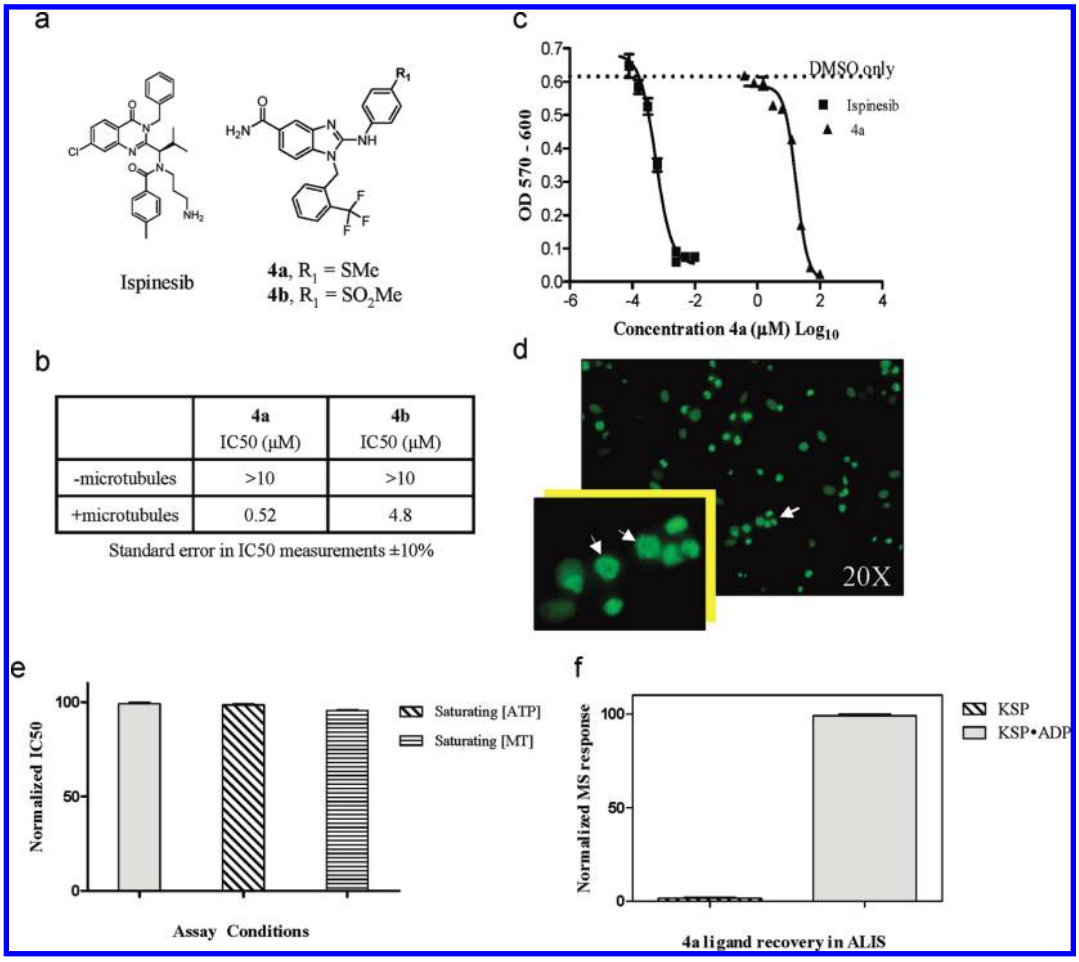

FIGURE 1: Biochemical and biological activities of benzimidazole compounds **4a** and **4b**. (a) Chemical structure of Ispinesib (left) and series **4** representative compounds **4a** and **4b** (right). (b) Inhibition of KSP ATPase activity by compounds **4a** and **4b** in the presence and absence of microtubules. (c) Effect of Ispinesib (■) and compound **4a** (▲) as single agents on the proliferation of A2780 cells. Growth inhibition IC_{50} of 0.56 ± 0.05 nM and 17 ± 3 μM were determined by Alamar Blue assays for Ispinesib and compound **4a**, respectively, as described in Experimental Procedures. (d) Monoaster formation was observed in HeLa-GFP cells at 50 μM compound **4a** after 18 h incubation. (e) Relative IC_{50} values for compound **4a** under limiting (100 μM ATP, 0.2 μM microtubules) and saturating ATP (1 mM) and microtubule (10 μM) concentrations. The IC_{50} measured at 100 μM ATP and 0.2 μM microtubule concentration was set at 100% for normalization. (f) Binding of compound **4a** in the ALIS system as determined by the recovery of the ligand from the dissociation of the protein−ligand complex from reversed-phase chromatography in the presence and absence of ADP. The data are shown as normalized mass spectrometry signal response.

Affinity selection−mass spectrometry (AS-MS) techniques including the proprietary automated ligand identification system (ALIS) (*16*, *17*) have received recent attention as a way to screen proteins for ligands in an unbiased manner and theoretically enable the discovery of compounds that bind at both precedented and unprecedented sites. The ALIS platform screening conditions were configured to enable the detection of both ADP competitive and ADP uncompetitive compounds to enable the capture of the broadest range of ligand series for KSP inhibition. Among the hit series, the most notable were based on the benzimidazole series such as compounds **4a** and **4b** (Figure 1a). Kinetic analysis of the inhibition of ATPase activity and further mechanistic studies using temperature-dependent circular dichroism (TdCD) confirmed **4a** and **4b** binding in the presence of saturating ADP and Ispinesib concentrations, implying existence of a novel druggable binding pocket in KSP. Interestingly, cell-based studies showed that the combination of compound **4a** and Ispinesib was additive, in agreement with the TdCD results. Targeting this novel site in KSP with potent inhibitors provides additional avenues for addressing issues related to Ispinesib resistance that has been described in the current literature (*14*, *18*).

EXPERIMENTAL PROCEDURES

Materials. Ispinesib was synthesized at the Merck Research Laboratories as the active (*R*) enantiomer. Its identity was confirmed by NMR and LC-MS. Series **4** compounds were synthesized accordingly to previously published methods and were characterized using LC-MS (*19*).

Expression and Purification of KSP Motor Domains, Wild Type, and D130V and A133D Mutants. The KSP proteins were purified as previously described (*20*). Briefly, the motor domain of KSP (amino acids 15−368) was cloned into pET24a for bacterial expression as an N-terminal hexahistidine fusion protein. Site-directed mutagenesis was performed on pET24a-KSP to generate D130V and A133D mutations. The mutations were confirmed by DNA sequencing (Genewiz Inc.). The proteins were expressed in *Escherichia coli* BL21(DE3) (Novagen) cells for 4 h at 37 °C. The bacterial pellet was lysed in 50 mM Tris, pH 8.0, 300 mM NaCl, 10 mM imidazole, and 1 mL/L protease inhibitor cocktail III (EMD Biosciences). After microfluidizing, the lysate was clarified by ultracentrifugaton (100000*g* for 1 h at 4 °C) and loaded onto a Ni-NTA agarose column prequilibrated with lysis buffer. The protein was eluted with 0−250 mM imidazole gradient and was further purified with

an S200 gel-filtration column (GE Healthcare). Fractions which were >95% pure based on SDS−PAGE analyses were pooled. The purified (nucleotide-free) wild-type KSP was shown to be fully active in the ATPase assay. The concentrations of WT and mutant KSP were determined in 6 M GdnHCl using UV spectrophotometry and an extinction coefficient at 280 nm of 21200 M^{-1} cm^{-1} based on the amino acid sequence.

AS-MS Setup for ALIS Screening and K_d Measurements. The general size-exclusion chromatography (SEC) based AS-MS hardware configuration used in this study has been described previously (*16*, *17*). Briefly, this system uses continuous SEC to isolate protein−ligand complexes from unbound library members. Samples containing a target protein, protein−ligand complexes, and unbound compounds are injected onto an SEC column, where the complexes are separated from the nonbinding component by a rapid SEC step. SEC is performed at 4 °C using buffered saline, typically 50 mM, pH 7.5, phosphate buffer containing 150 mM NaCl. The eluant from the SEC column is passed through a UV detector (Agilent G1314A using a G1313 microflow cell) where the band containing the protein−ligand complex is identified by its native UV absorbance at 230 nm. After a pause to allow the band to leave the first detector and enter a valving arrangement, the protein−ligand complex peak is automatically transferred to a reversed-phase chromatography (RPC) column (Higgins Targa-C_{18}, 0.5 mm i.d. × 50 mm length; Higgins Analytical Inc.). Ligands are dissociated from the complex and trapped at the head of the RPC column, where they are desalted and eluted into the mass spectrometer using a gradient of 0%−95% acetonitrile (0.1% formic acid) in water (0.1% formic acid) over 5 min using an Agilent capillary binary pump (G1376A) for eluant delivery at 20 μL/min. To promote dissociation of ligands from the complex, the RPC column is maintained at 60 °C using an Agilent G1316A column compartment. In this study, MS analysis was performed using a Waters LCT "Classic" high-resolution time-of-flight mass spectrometer (Manchester, U.K.) with positive-mode ionization occurring from a standard nebulized electrospray ionization (ESI) source with the capillary at 3.5 kV, a desolvation temperature of 180 °C, a source temperature of 100 °C, and 30 V "cone" and 3 V extraction lens settings. For this program we optimized the ALIS screening conditions to capture both ATP competitive and noncompetitive series, with the optimal [ATP] of 3.3 μM determined by titration (data not shown). Ion current detection of ligand at expected mass was used to quantify the bound and free forms observed in the AS-MS setup. Prior calibration was performed by injecting varying concentrations of ligands in the binding buffer (20 mM PIPES, pH 6.8, 300 mM NaCl, 0.5 mM ADP, 2 mM $MgCl_2$, and 1 mM DTT). The experiments were conducted with and without 300 μM Ispinesib, the concentration which was deemed as saturating under the AS-MS setup. The experimentally determined bound and free fractions were fitted to the Scatchard equation for determination of binding constant (K_d) and stoichiometry (n) assuming equivalent noninteracting sites.

KSP in Vitro End Point Assay. For the determination of KSP *in vitro* enzymatic activity, an end point assay format was used based on the colorimetric detection of hydrolyzed ATP. In brief, the purified KSP motor domain protein was incubated in kinesin buffer (80 mM Na-PIPES, pH 6.9, 1 mM $MgCl_2$, 1 mM EGTA) for 10 min at room temperature in the presence of 0.2 μM preformed, taxol-stabilized microtubules (Cytoskeleton Inc., catalog no. MT001-XL; prepared according to manufacturer's recommendations) in the presence or absence of small molecule candidate inhibitors (final DMSO concentration held constant at 2%) in a reaction volume of 22.5 μL. Following the preincubation step, the microtiter plates are centrifuged briefly in a tabletop centrifuge prior to addition of 2.5 μL of a 1 mM ATP stock solution, which initiates the enzymatic reaction. After 1 h incubation at room temperature, the reaction was stopped by addition of 50 μL of Biomol Green reagent (Biomol International Inc.). Following a 20 min incubation at room temperature, the plate is transferred to a spectrophotometer, and the absorbance at 620 nm is measured. The signal is proportional to the level of free phosphate in solution, which is a direct consequence of KSP's ATP hydrolyzing activity. Signal is plotted against inhibitor concentration, and a sigmoidal dose response is analyzed using ActivityBase software (IDBS Inc.) to determine corresponding IC_{50} values. For IC_{50} determination at saturation substrate concentrations, the assay conditions were kept the same except either the ATP concentration was increased to 1 mM or the microtubule concentration was increased to 10 μM. ATPase activity in the absence of microtubules was measured similarly but with higher concentration of KSP (200 nM final concentration).

Kinetics of KSP Inhibition by Benzimidazoles. ATPase activity was determined by a continuous spectrophotometric assay based on oxidation of NADH coupled to ADP through pyruvate kinase and lactate dehydrogenase (*21*). The level of NADH was monitored by observing the decrease in absorbance at 340 nm. The reaction was performed in a cuvette maintained at 25 °C and containing 10 nM of the same KSP wild-type enzyme construct used for the end point assay, in the same buffer at pH 7.2, in addition to 20 units/mL lactate dehydrogenase, 10 units/mL pyruvate kinase, 2 mM phosphoenolpyruvate, 0.15 mM NADH, and ATP concentration ranging from 7.5 to 270 μM. Inhibition by compound **4a** was assessed using 4, 8, 16, and 32 μM added from DMSO stock solution so the final DMSO concentration in the reaction mixture remains constant at 2%. Initial velocities under steady-state condition were determined in duplicate using a $\Delta\varepsilon_{340}$ of 6.22 nM^{-1} cm^{-1}, resulting in data points with an average of 4% deviation from the mean. Nonlinear regression fitting to Michaelis−Menten equations for competitive, noncompetitive, uncompetitive, and mixed inhibition was accomplished with GraphPad Prism (GraphPad Software Inc.).

Alamar Blue Cell Proliferation Assay. A2780 cells were plated at 1×10^4/100 μL of media per well in 96-well tissue culture dishes in the following media: 10% FBS, DMEM, 1% penicillin/streptomycin glutamine, 1% nonessential amino acids, 1% sodium pyruvate, and 1% HEPES buffer. One column in the plate was left without cells to act as negative control. Once plated, the cells were placed in a 37 °C tissue culture incubator for 3−4 h to allow cells to adhere. Compounds were added in a 10-point, one-half log titration to all plates. Each titration series was performed in triplicate, and a constant DMSO of 0.1% was maintained throughout the assay. Control of 0.1% DMSO was also included. Each compound dilution series was made in media without serum. After the addition of the compound, the plate was incubated at 37 °C for 42 h. Twenty microliters of Alamar Blue staining reagent was added to each sample and control well on the titration plate, and the plate was returned to incubation at 37 °C. Alamar Blue fluorescence was analyzed 6 h later utilizing the SpectraMax reader using 530−560 nm wavelength excitation and 570−600 nm emission. A cytotoxic EC_{50} was derived by plotting

compound concentration on the *x*-axis and fluoresence reading for each titration point on the *y*-axis. The data were fitted to the sigmoidal dose−response model using GraphPad Prism (GraphPad Software Inc.) to calculate the cytotoxic EC_{50} at 95% confidence level.

Immunofluoresence Staining. HeLa-GFP cells were seeded at $1 \times 10^4/100\ \mu L$ of media per well of a 96-well plate in DMEM medium with 10% FBS, 1% penicillin/streptomycin glutamine, 1% nonessential amino acids, 1% sodium pyruvate, and 1% HEPES buffer leaving one column without cells to act as negative control. The plate is left at 37 °C in a tissue culture incubator for 3−4 h to allow cells to attach. An equal volume of media containing either DMSO (control) or fixed concentration of **4a** is added to cells. After the addition of the compound, the plate is incubated at 37 °C for 4 h. Immunofluoresence staining of α-tubulin and chromatin in HeLa-GFP cells was used to examine the cytology of cells with and without **4a**. Monoastral spindles were observed in **4a**-treated cells. Immunostained samples were imaged on an inverted microscope. Images shown are maximum intensity projections of deconvoluted stacks.

Temperature-Dependent Circular Dichroism (*TdCD*). The thermal denaturation studies were performed as previously described with slight modifications (*20*). Briefly, ellipticity was monitored at 230 nm as a function of temperature with a 1 mm path-length cell. The thermal scan rate was 0.5 °C/min with a 4 s response time and 30 s equilibration between measurements. Stock protein was diluted to 8−10 μM with 20 mM PIPES, pH 6.9, 300 mM NaCl, 1 mM $MgCl_2$, and 1 mM DTT. The binding of benzimidazole series of compounds was tested in the presence of 500 μM ADP with and without 100 μM Ispinesib as indicated in individual experiments. The final DMSO concentration was 2% for the TdCD experiments with Ispinesib and compounds present. Data were analyzed using the Jasco software to calculate protein melting temperatures (T_m) and the enthalpy of unfolding ΔH_u. The protein melting temperatures were reported from two or three separate experiments.

The relationship between ligand binding and protein stability as detected by changes in the midpoint of unfolding (T_m) has been well documented (*22*, *23*), and K_d values can be estimated from the ΔT_m determined by temperature-dependent circular dichroism (TdCD) (*24*). Equation 1 (*24*) was used to calculate K_d values for Ispinesib and monastrol binding to WT and mutant forms of KSP. The ligand binding constant ($K_L(T)$) can be calculated at any temperature (T) by the equation:

$$K_L(T) = K_L(T_m)\exp\left\{\left(\frac{-\Delta H_L(T)}{R}\right)\left(\frac{1}{T}-\frac{1}{T_m}\right) + \left(\frac{\Delta C_{pL}}{R}\right)\left[\ln\frac{T}{T_m}+1-\frac{T}{T_m}\right]\right\} \quad (1)$$

where T_m is the midpoint of unfolding in the presence of ligand, ΔH_L is the enthalpy of binding, ΔC_{pL} is the ligand binding heat capacity, and $K_L(T_m)$ is the ligand binding constant at T_m. If estimates for both ΔH_L and ΔC_{pL} are available, then the ligand binding constant, $K_L(T)$, can be calculated at any temperature T (assuming that the heat capacity term is temperature independent). $K_L(T_m)$ can be calculated by the equation:

$$K_L(T_m) = \{\exp\{-(\Delta H_u(T_0)/R)(1/T_m - 1/T_0) + (\Delta C_{pu}/R)[\ln(T_m/T_0)+(T_0/T_m)-1]\}-1\}/[L_{T_m}] \quad (2)$$

where T_0 is the midpoint of unfolding for the unliganded protein, T_m is the midpoint of unfolding in the presence of ligand, ΔH_u is the enthalpy of protein unfolding, ΔC_{pU} is the heat capacity associated with protein unfolding, and $[L_{T_m}]$ is the free concentration of ligand at T_m. Unless otherwise specified, ΔH_L values were assumed to be −7 kcal/mol, where data were unavailable, and ΔC_{pL} was set to zero for TdCD-determined $K_L(T)$.

RESULTS AND DISCUSSION

*Identification of **4a** and **4b** and Their Biochemical and Biological Activity*. In an effort to discover KSP inhibitors with novel mechanism of action, automated ligand identification system (ALIS) technology was deployed to screen the KSP·ADP complex. ALIS is an affinity selection mass spectrometry platform for label-free, high-throughput screening of mixture-based combinatorial libraries. The KSP·ADP complex screening campaign involved incubation of the KSP·ADP complex with mass-encoded combinatorial libraries followed by automated microscale size-exclusion chromatography. Compounds that bound to the KSP·ADP complex were dissociated from the enzyme during subsequent reversed-phase HPLC, analyzed by mass spectrometry, and identified according to appropriate mass information embedded in each library. Our high-throughput screening effort resulted in identification of benzimidazole-based ligands with a range of binding affinities. The preliminary biochemical activities of some of these compounds including compounds **4a** and **4b** (Figure 1a) have been evaluated previously (*19*).

Briefly, compounds **4a** and **4b** were found to reproducibly inhibit microtubule-stimulated KSP ATPase activity with IC_{50} of 0.52 and 4.8 μM, respectively (Figure 1b). Compounds in this series have also been tested against a panel of kinesins and, in general, were very selective; for example, both **4a** and **4b** were inactive ($IC_{50} > 50\ \mu M$) against both Kif3B and nKHC, with smaller selectivity ratios noted for HSET in an end point biochemical assay (10× for **4a**, 5× for **4b**) (*19*). Both compounds also exhibited activity as single agent in cell proliferation assay (representative **4a** results shown in Figure 1c and ref *19*). Compound **4a** inhibited proliferation of the human ovarian tumor cell line A2780 with an EC_{50} of 17 ± 3 μM after 7 days of treatment (Figure 1c) in comparison to the more potent Ispinesib control (EC_{50} = 0.56 ± 0.05 nM) assayed under the same conditions. Both **4a** and **4b** were tested in a phenotypic monoaster formation microscopy experiment, and monasters were visually apparent at both 25 and 50 μM **4a** (Figure 1d) concentrations and at 50 and 100 μM **4b** concentrations (data not shown). In parallel to the activity optimization and SAR generation (*19*), we sought additional mechanistic insights into the inhibition profile as a way to differentiate our series from the other reported KSP chemotypes.

KSP exhibits a basal ATPase activity in the absence of microtubules although the k_{cat} for this reaction is ~250-fold slower than in the presence of microtubules. In order to more fully understand the properties of the newly identified benzimidazole class of KSP inhibitors, compounds **4a** and **4b** were tested as inhibitors of the basal ATPase activity. As seen in Figure 1b, while the compounds showed some inhibition of the activity at the highest concentration tested, their potency was >2−19-fold lower than that observed in the presence of microtubules. Upon varying the ATP concentrations and microtubule concentrations to saturating levels, we observed no significant (<5%) corresponding change in the IC_{50} of compounds **4a** and **4b**, implying

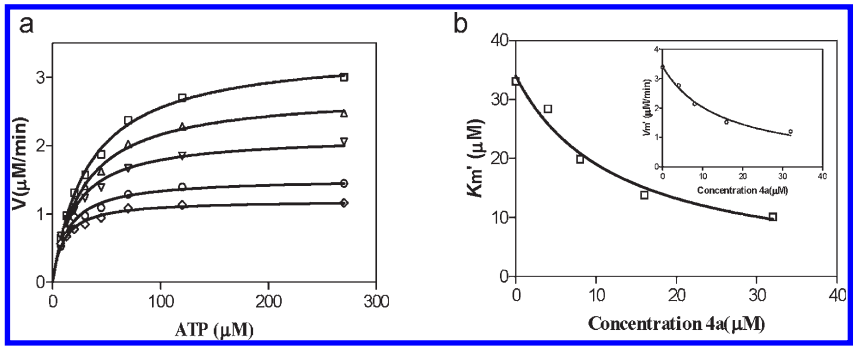

FIGURE 2: Steady-state kinetics of KSP ATPase inhibition by compound **4a**. (a) Plots of ATPase initial velocities versus ATP concentration and in the presence of 0 (□), 4 (△), 8 (▽), 16 (○), and 32 (◇) μM compound **4a**. Nonlinear regression fit using the Michaelis−Menten equation for zero inhibitor concentration resulted in K_m and V_m of 33 ± 1.8 and 3.4 ± 0.06 μM/min, respectively. Variations in both K_m' and V_m' were observed in the presence of increasing concentration of compound **4a**. (b) Plots of K_m' (□) and V_m' (○) (inset) versus concentration of compound **4a**. Nonlinear regression fit to $K_m' = K_m/(1 + [\mathbf{4a}]/K_i)$ and $V_m' = V_m/(1 + [\mathbf{4a}]/K_i)$ resulted in K_i of 12.7 ± 2.2 and 14.7 ± 1.6 μM, respectively. The overall results are consistent with uncompetitive inhibition with respect to ATP.

that the compounds do not directly bind to either the nucleotide or the microtubule binding sites in KSP (Figure 1e). Since ADP and $MgCl_2$ were included in the ALIS screening setup, we investigated whether the binding of the compounds was dependent on the nucleotide. In the ALIS system, we observed the recovery of KSP-bound **4a** was contingent upon the presence of nucleotide in the assay buffer (Figure 1f). To more fully understand the nucleotide dependence on binding of **4a**, we measured steady-state inhibition kinetics for **4a** at saturating microtubule concentration.

Inhibition of Steady-State ATPase Activity in the Presence of Saturating Concentration of Microtubules. Inhibitors of KSP ATPase activity could be classified according to their mode of inhibition with respect to ATP as substrate. Compounds that bind to the induced-fit loop L5 (monastrol/Ispinesib) site (*5*, *25*, *26*) exhibit typical uncompetitive behavior in steady-state kinetic studies and include diverse chemotypes that are not necessarily related to the quinazolinone core of Ispinesib or to the 2-thiopyrimidine core of monastrol (*27*). Competitive inhibitors have been shown by mutagenesis and molecular modeling studies to map either to the nucleotide binding site (e.g., the thiazole series (*28*)) or to an allosteric site distant from the ATP site and located in a cleft defined by helices α4 and α6 (e.g., biaryl type (*14*)). Many other inhibitors containing, for example, the thienoquinoline, triazine, triazolopyrimidune, and pyridine cores have been reported without defined mechanism of inhibition (*27*). As shown in Figure 2, our 2-amino benzimidazole compound **4a** inhibited KSP ATPase activity uncompetitively as evidenced by both K_m and V_m varying in concert by a factor of $(1 + [\mathbf{4a}]/K_i)$ in the presence of inhibitor. Compound **4a** clearly exhibited a preference for binding to the nucleotide-bound KSP (ESI complex) in agreement with the ALIS experiments. The uncompetitive behavior with respect to ATP excludes the possibility that compound **4a** binds at not only the nucleotide site but also the allosteric site between helices α4 and α6 previously identified for the biaryl inhibitors. The overall ALIS and enzyme inhibition data support binding to either the induced-fit loop L5 (Ispinesib/monastrol) site or a novel hitherto unknown KSP inhibitor site. We sought confirmation for either alternative through further binding studies based on circular dichroism and thermal denaturation of KSP in the presence of various combinations of ligands, including Ispinesib.

*Binding of **4a** and **4b** to KSP·ADP and KSP·ADP·Ispinesib Complexes Using Temperature-Dependent Circular Dichroism (TdCD)*. In TdCD, the loss of protein secondary structure was monitored as a function of temperature. Proteins bound with ligand become more resistant to thermal unfolding compared to the unliganded protein because of the additional stabilization interactions created between the ligand and the protein. It is well documented that the increase in the midpoint of unfolding (T_m) in the presence of a ligand is proportional to the affinity of the ligand (*23*, *29*). These studies have also demonstrated that dissociation constants (K_d) can be estimated

Table 1

Compound	Structure	Single agent ΔT_m (°C)	Combination ΔT_m (°C)	Single agent TdCD K_d[a] (μM)
4a	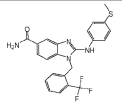	4.3 ± 0.1	2.5 ± 0.1	2
4b	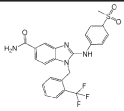	3.9 ± 0.1	2.2 ± 0.14	2.5
4c	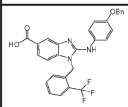	2.0 ± 0.14	0.8 ± 0.1	14
4d	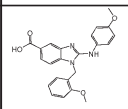	3.1 ± 0.2	1.3 ± 0.1	5
4e	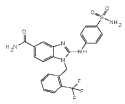	5.8 ± 0.2	2.6 ± 0.1	0.6
4f	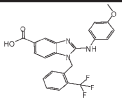	4.9 ± 0.1	2.5 ± 0.1	1.2
4g	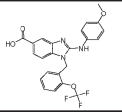	3.6 ± 0.1	1.4 ± 0.08	3.4

[a]Assuming ΔH_u = 100000 cal/mol and ΔH_L = −7000 cal/mol. Standard error values are from two to three experiments. Single agent refers to binding of series **4** compound to the binary [KSP·ADP] whereas combination refers to the ternary [KSP·ADP·Ispinesib] complexes. The TdCD experiments were performed as described in Experimental Procedures and in the legend of Figure 3.

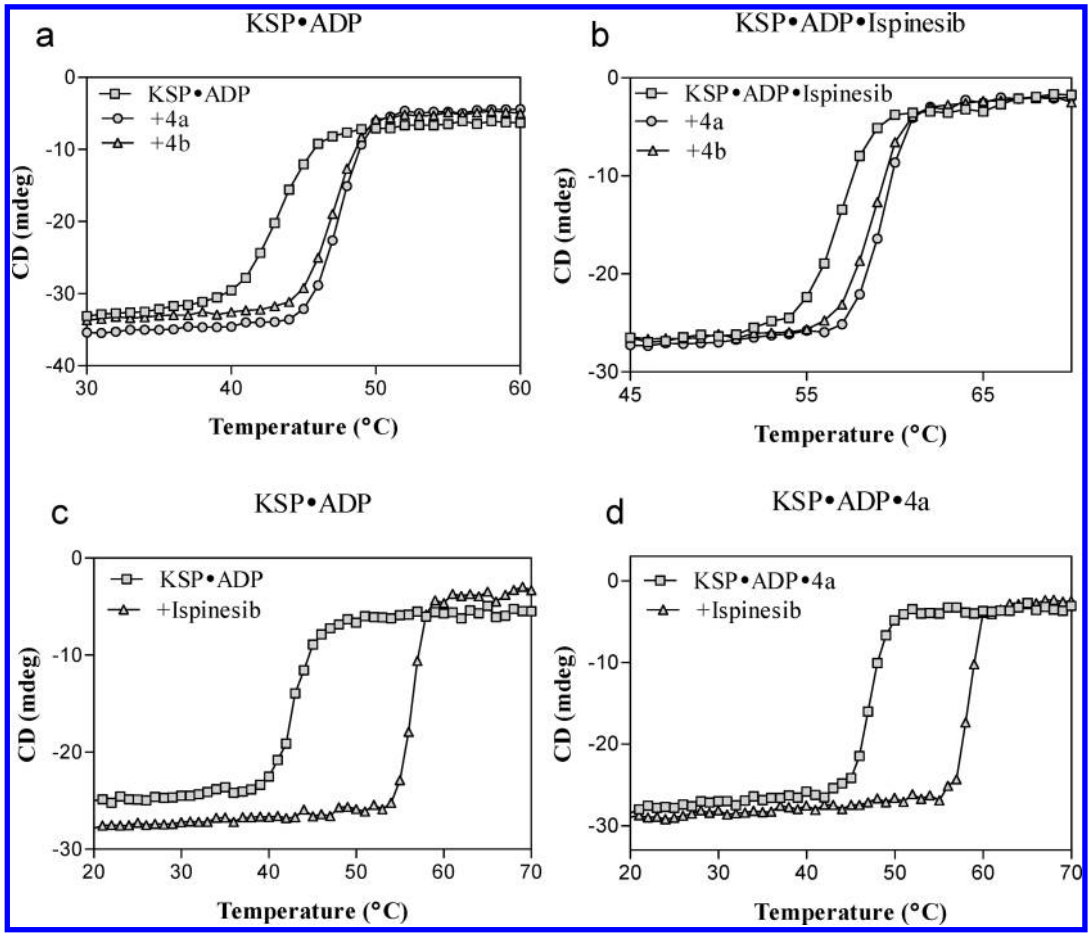

FIGURE 3: TdCD analyses of **4a** and **4b** binding to KSP·ADP and KSP·ADP·Ispinesib. (a) CD thermal denaturation curves for WT KSP·ADP (□); + compound **4a** (△); compound **4b** (○). (b) CD thermal denaturation curves for WT KSP·ADP·Ispinesib (□); + compound **4a** (△); compound **4b** (○). (c) CD thermal denaturation curves for WT KSP·ADP (□); + Ispinesib (△). (d) CD thermal denaturation curves for WT KSP·ADP·**4a** (□); + Ispinesib (△). Ellipticity (mdeg) was measured at 230 nm as a function of temperature (22−75 °C). Protein concentrations were 10−12 μM, ADP concentration was saturating at 0.25 mM, and the concentration of the inhibitors was 100 μM in 20 mM PIPES, pH 6.9, 300 mM NaCl, 1 mM $MgCl_2$, 1 mM DTT, and 1% DMSO. The temperature was increased at 1 °C/min in a 1 mm path-length quartz cuvette.

from ligand-induced changes in the T_m measured by methods such as differential scanning calorimetry or TdCD. TdCD recapitulated the ALIS results for the binding of the series **4** compounds to the KSP·ADP complex. No significant T_m shift in the apo KSP melting was observed in the presence of the compound, consistent with the preferential binding of **4a** to the KSP·ADP complex (data not shown). Compounds tested in the presence of saturating levels of ADP/Mg^{2+} demonstrated ΔT_m of 2−5.8 °C when tested using TdCD, using the equation (Table 1):

$$\text{single agent } \Delta T_m(\text{compd}) = T_m(\text{KSP·ADP·compd}) - T_m(\text{KSP·ADP})$$

In the presence of 100 μM **4a** and **4b**, the KSP·ADP form showed 4.3 ± 0.1 and 3.9 ± 0.1 °C ΔT_m (Figure 3a, Table 1). The calculated TdCD K_ds for **4a** and **4b** were 2 and 2.5 μM, respectively. Compound **4e** with SO_2NH_2 at the R1 position had the largest ΔT_m (5.8 ± 0.2 °C) among the series **4** panel of compounds tested. The SAR at the three variable "R" groups was relatively flexible; however, several trends were evident (Table 1). For the R1 position heteroatom-containing groups proved to be preferred, and a range of groups were found to be active. However, groups larger than a few atoms, such as the benzyloxy group, proved to be less capable of stabilizing the protein in both of its forms. At the R2 position the electron-withdrawing trifluoromethyl group (such as **4f**, ΔT_m = 4.9 ± 0.1, 2.5 ± 0.1 °C) was preferred over the more electron-donating methoxy group (**4d**, ΔT_m = 3.1 ± 0.2, 1.3 ± 0.1 °C), and the trifluoromethoxy group with intermediate electronic properties was also intermediate in its ability to stabilize the protein (**4g**, ΔT_m = 3.6 ± 0.1, 1.4 ± 0.08 °C), both as a single agent and in combination. The R3 position favored small hydrogen bond acceptors such as the primary amide and carboxy-containing moieties.

The KSP inhibitor, Ispinesib, has been shown to be uncompetitive with ATP, and the thermodynamic basis of Ispinesib binding has been recently investigated (*20*). A TdCD experiment was designed to determine whether the series **4** compound-induced T_m stabilization observed in the KSP·ADP complex (as single agents) can also observed in the KSP·ADP·Ispinesib complex. Ispinesib binding to KSP·ADP resulted in a large (~12 °C) T_m shift consistent with the expected single-digit nanomolar affinity for the compound (Figure 3c). Incubation of the compounds with the KSP·ADP·Ispinesib complex resulted in additional stabilization of 0.8−2.6 °C (Figure 3b, Table 1). Addition of Ispinesib to a preformed KSP·ADP·**4a** complex resulted in additional large (~12 °C) T_m shifts consistent with the formation of a KSP·ADP·**4a**·Ispinesib complex (Figure 3d). The affinity rank order for the series **4** compounds was largely conserved between the Ispinesib-bound (KSP·ADP·Ispinesib) and Ispinesib-unbound (KSP·ADP) forms of KSP (Table 1). However, the

series **4**-induced ΔT_ms in the KSP·ADP·Ispinesib complex were lower than the ΔT_ms observed in the absence of Ispinesib (Table 1), implying lower TdCD affinity for the series **4** compounds in the KSP·ADP·Ispinesib complex compared to the KSP·ADP complex. Possibly the conformational change induced by Ispinesib could negatively affect the affinity of the KSP·ADP·Ispinesib complex for compound **4a**. However, it could also be speculated that the differences in the **4a**-induced stabilization could be due to the inherent limitations of the TdCD temperature-stabilization technique. The net change in stabilization from the combination of Ispinesib with **4** series compounds was calculated below. A summary of select single agent and combination T_ms is reported in Table 1.

$$\text{combination } \Delta T_m(\text{compd}) = T_m(\text{KSP·ADP·Ispinesib·compd}) - T_m(\text{KSP·ADP·Ispinesib})$$

*Binding of **4a** to KSP·ADP and KSP·ADP·Ispinesib Complexes As Determined by AS-MS*. Preliminary quantitative AS-MS experiments (data not shown) indicated that the series **4** inhibitors also bound to the KSP·ADP·Ispinesib complex. Using known amounts of compound **4a** to calibrate the AS-MS system, we determined quantitatively its binding to either KSP·ADP or the ternary KSP·ADP·Ispinesib complex. The results illustrated in Figure 4 indicated that addition of a 6−7-fold excess of Ispinesib over KSP failed to alter the binding affinity of compound **4a** for KSP·ADP. The two dissociation constants derived from Scatchard analyses were practically the same within experimental error, 8.8 ± 1.8 μM for KSP·ADP versus 9.4 ± 1.3 μM for KSP·ADP·Ispinesib. The results are consistent with binding of compound **4a** to KSP at a distinct nonoverlapping site with respect to Ispinesib and support in part the results from the TdCD experiments.

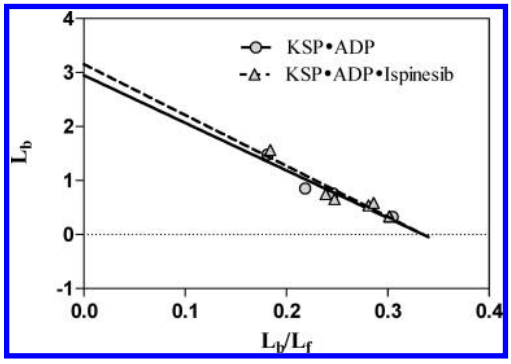

FIGURE 4: AS-MS analyses of **4a** binding to KSP·ADP and KSP·ADP·Ispinesib. **4a** was added at variable concentrations from 1 to 10 μM to 4 μM KSP in binding buffer containing 20 mM PIPES, pH 6.8, 300 mM NaCl, 1 mM $MgCl_2$, 1 mM DTT, and 0.25 mM ADP in the absence (○) or in the presence of 40 μM Ispinesib (△). The mixtures were incubated for 30 min at room temperature and then injected into the AS-MS system as described in the Experimental Procedures for determination of bound **4a** (L_b) and free **4a** (L_f). The results were fitted to the Scatchard equation $L_b = -K_d(L_b/L_f)$, where P is the total KSP concentration and n and K_d are the stoichiometry of binding and dissociation constant, respectively. In the absence of Ispinesib K_d = 8.8 ± 1.8 μM and nP = 2.9 ± 0.43 μM and in the presence of Ispinesib K_d = 9.4 ± 1.3 μM and nP = 3.2 ± 0.34 μM.

*Binding of **4a** to Ispinesib-Resistant Mutants D130V and A133D using TdCD*. To further probe the mechanism of binding of series **4** compounds, the TdCD studies were also performed for the two Ispinesib-resistant mutants D130V and A133D (*14*, *18*). These mutant proteins can be used to probe the binding site overlap between Ispinesib and series **4** compounds. Residues A133 and D130 happen to be near the base of the L5 loop, which is known to undergo major conformational rearrangement upon inhibitor binding. Both residues D130 and A133 are engaged in extensive hydrogen bond network between each other and the neighboring residues that form the induced-fit binding pocket for Ispinesib and monastrol. The hydrogen bond network extending from D130 and A133 seems to hold the key to the architecture required for binding of Ispinesib and monastrol (*20*). Both mutants have been shown to have >1000-fold lower Ispinesib binding affinity (*20*).

In the presence of 100 μM compound **4a**, the A133D·ADP complex showed a 4.6 ± 0.14 °C stabilizing shift in the T_m relative to the "apo" A133D·ADP complex (Figure 5a). Consistent with the A133D data, the TdCD experiments using the D130V·ADP complex showed increase in the ΔT_m of 2.9 ± 0.1 °C, implying that series **4** bind to both the Ispinesib-resistant mutant forms of KSP (Figure 5b). The A133D·ADP and D130V·ADP TdCD binding affinity for **4a** was 1.5 and 5 μM, comparable to their WT KSP·ADP counterpart (Figure 5; Table 2). Furthermore, the double mutant of A133D + D130V, in the presence of ADP, was also shown to retain the binding affinity for compound **4a** (TdCD K_d = 2 μM, Table 2) comparable to the WT KSP protein (Figure 5c). In contrast, Ispinesib and monastrol have been

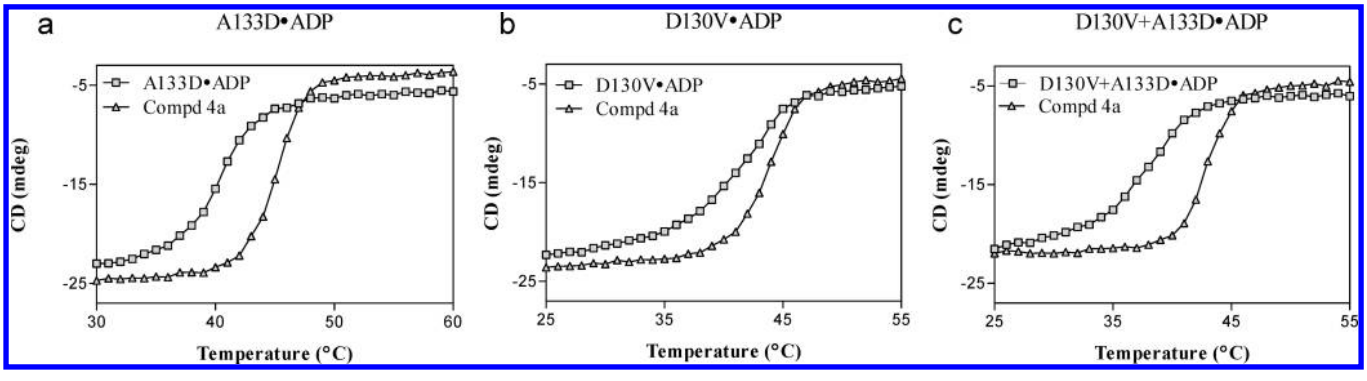

FIGURE 5: TdCD analyses of **4a** and **4b** binding to Ispinesib-resistant KSP, A133D, D130V, and A133D + D130V. (a) CD thermal denaturation curves for A133D·ADP (□); + compound **4a** (△). (b) CD thermal denaturation curves for D130V·ADP·Ispinesib (□); + compound **4a** (△). (c) CD thermal denaturation curves for D130V + A133D·ADP·Ispinesib (□); + compound **4a** (△). Ellipticity (mdeg) was measured at 230 nm as a function of temperature (22−75 °C). Protein concentration was 10−12 μM, ADP concentration was saturating at 0.25 mM, and inhibitor concentration was 100 μM in 20 mM PIPES, pH 6.8, 300 mM NaCl, 1 mM DTT, and 1% DMSO. The temperature was increased at 1 °C/min in a 1 mm path-length quartz cuvette. The ΔT_m values and the calculated TdCD K_d values are shown in Table 2.

Table 2

	A133D·ADP		D130V·ADP		A133D + D130V·ADP	
compd	ΔT_m (°C)	TdCD K_d[a] (μM)	ΔT_m (°C)	TdCD K_d[a] (μM)	ΔT_m (°C)	TdCD K_d[a] (μM)
4a	4.6 ± 0.14	1.5	2.9 ± 0.1	5	4.4 ± 0.2	2

[a]Assuming ΔH_u = 100000 cal/mol and ΔH_L = −7000 cal/mol. Standard error values are from two to three experiments.

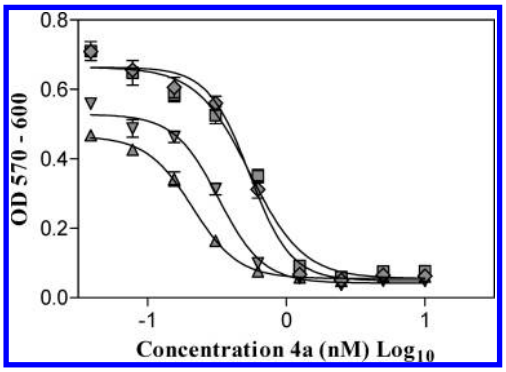

FIGURE 6: Potency of Ispinesib in the presence of compound **4a**. Ispinesib was added at increasing concentration to A2780 cells untreated (□) or pretreated with three different concentrations, 1 (◇), 5 (▽), and 10 (△) μM, of compound **4a**. Cells were preincubated with the compound for 4 h before addition of Ispinesib. Cytotoxic EC_{50} was determined by Alamar Blue staining and calculated as mentioned in the Experimental Procedures. EC_{50} values for Ispinesib alone and titrated in the presence of 1, 5, and 10 μM compound **4a** were 0.55 ± 0.08, 0.54 ± 0.06, 0.33 ± 0.03, and 0.21 ± 0.03 nM, respectively.

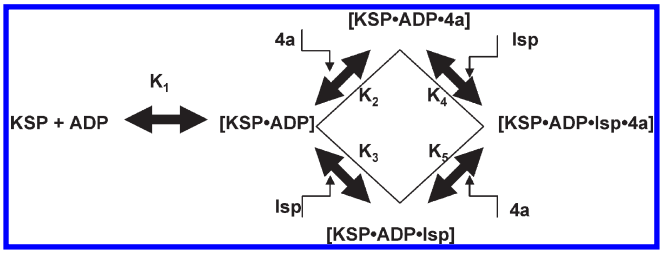

FIGURE 7: Equilibrium binding model for KSP, ADP, Ispinesib, and compound **4a**. Based on the TdCD and AS-MS analyses, a model for thermodynamic equilibrium between KSP, ADP, Ispinesib, and **4a** is depicted. Both **4a** and Ispinesib bind preferentially to the KSP·ADP bound form of the protein. **4a** can also bind to the KSP·ADP·Ispinesib bound form of KSP.

shown to bind D130V and A133D mutants with >1000-fold lower affinity (*20*). Thus, the TdCD results demonstrated that there is no significant difference (<2-fold) in the **4a** binding affinity of Ispinesib-resistant mutants compared to their WT counterpart, implying an existence of a unique binding site for benzimidazole series **4**. The available data clearly indicate that compound **4a**, which inhibits ATPase uncompetitively, binds to a novel site distinct from Ispinesib and hitherto unknown.

*Cell-Based Potency of Ispinesib in the Presence of **4a**.* Given the results of the AS-MS studies, the steady-state kinetics of ATPase inhibition, and TdCD binding studies, we sought to investigate the outcome of the combined effect of compound **4a** and Ispinesib in cell-proliferation assays (Figure 6). The EC_{50} value derived from the titration of Ispinesib alone in the ovarian tumor cell line A2780 was 0.55 ± 0.08 nM. In the presence of 1, 5, and 10 μM compound **4a** the potency of Ispinesib increased as evidenced by the corresponding decrease in EC_{50} of 0.54 ± 0.06, 0.33 ± 0.03, and 0.21 ± 0.03 nM. Using the additivity rule for drug combination (*30*, *31*) the theoretical EC_{50} values could be calculated as 0.52, 0.39, and 0.24 nM, respectively. They are in close agreement with the experimentally derived values, indicating that in cell proliferation assays the combined effect of Ispinesib and compound **4a** is additive. Since resistance to Ispinesib occurs quite readily (*14*, *18*), the discovery of novel chemotypes that bind at distinct sites on KSP and act additively or synergistically remains imperative. Further characterization of the series **4** binding site especially by X-ray crystallography is critical for structure-based design to increase potency and selectivity. Other mechanistic aspects such as effect on interaction with microtubules and ADP cycling from the nucleotide binding site are also of interest and will be the subject of future studies.

CONCLUSION

A series of 2-aminobenzimidazoles (**4**) was originally discovered by affinity selection−mass spectroscopy using KSP in the presence of ADP. The series was subsequently found to be active in counter screen using end point ATPase and ovarian tumor cell (A2780) proliferation inhibition assays. The antimitotic effect reflecting in-cell KSP inhibition was also confirmed in immunofluorescence studies of dividing Hela-GFP in the presence of two representative compounds **a** and **b** from series **4**.

Many inhibitors of KSP ATPase have been reported in the literature, and several prototypes, e.g., Ispinesib, SB-743921, AZ4877, and MK-0731, have reached phase I/II clinical trials. The novel 2-aminobenzimidazole series **4** must be placed in the context of the established agents in terms of specific binding site, mechanism of inhibition, and ultimately clinical utility as selective antimitotic for cancer therapy. To that effect we demonstrated that these compounds inhibited ATPase activity uncompetitively like the induced-fit L5 loop inhibitors originally exemplified by Ispinesib and monastrol. Both AS-MS and TdCD data supported the uncompetitive mechanism, indicating preferential binding of inhibitor to enzyme−substrate to form the ternary enzyme−substrate−inhibitor (ESI) complex. Interestingly, however, binding studies by TdCD using wild-type KSP as well as Ispinesib mutants (A133D, D130V, and A133D + D130V) further indicated that series **4** compounds and Ispinesib do not share the same binding site at loop L5 and that both could together bind [KSP·ADP] to form the [KSP·ADP·Ispinesib·**4a**] quaternary complex as illustrated in Figure 7. The KSP binding site for the series **4** compounds is thus novel and distinct from all currently known inhibitor sites. It deserves further characterization at the molecular level, especially by X-ray crystallography. The measured IC_{50} difference for **4a** between the basal ATPase assay and the MT-stimulated ATPase assay implies that the microtubules could modulate the binding affinity of the compound to **4a**. The precise effect of series **4** compounds on microtubule interaction and ATPase activation remains to be investigated, although based on our IC_{50} results at saturating microtubule concentration, it is unlikely that the series **4** compounds bind to the microtubule binding site in KSP.

Finally, in ovarian tumor cell-proliferation studies, we demonstrated that the combination of series **4** compounds and Ispinesib is additive. These 2-aminobenzimidazoles are novel additions to the expanding family of KSP inhibitors. Further chemical optimization could lead to more potent and selective antimitotics that are clinically useful as single agent or in combination with other modalities to enhance cancer cell killing effect and to overcome resistance. Affinity-based screening technology such as AS-MS used in this study has the potential for wider application to many other drug targets. It was found to be most effective for discovery of allosteric inhibitors when potent active site masking agents are included in the screening paradigm.

ACKNOWLEDGMENT

We thank Dr. Andrew Prongay, Mr. Anthony Mannarino, and Ms. Polina Ogas for purifying the A133D, A133D + D130V (double mutant), and WT KSP constructs, respectively, and Dr. Huw Nash for helpful discussions.

REFERENCES

1. Miki, H., Okada, Y., and Hirokawa, N. (2005) Analysis of the kinesin superfamily: Insights into structure and function. *Trends Cell Biol. 15*, 467–476.
2. Sharp, D. J., Rogers, G. C., and Scholey, J. M. (2000) Microtubule motors in mitosis. *Nature 407*, 41–47.
3. Valentine, M. T., and Gilbert, S. (2007) To step or not to step? How biochemistry and mechanics influence processivity in kinesin and Eg5. *Curr. Opin. Cell Biol. 19*, 75–81.
4. Bergnes, G., Brejc, K., and Belmont, L. (2005) Mitotic kinesins: Prospects for antimitotic drug discovery. *Curr. Top. Med. Chem. 5*, 127–145.
5. Yan, Y., Sardana, V., Xu, B., Homnick, C., Halczenko, W., Buser, C. A., Schaber, M., Hartman, G. D., Huber, H. E., and Kuo, L. C. (2004) Inhibition of a mitotic motor protein: Where, how and conformational consequences. *J. Mol. Biol. 335*, 547–554.
6. Heald, R. (2000) Motor function in the mitotic spindle minireview. *Cell 102*, 399–402.
7. Sakowicz, R., Finer, J. T., Beraud, C., Crompton, A., Lewis, E., Fritsch, A., Lee, Y., Mak, J., Moody, R., Turincio, R., Chabala, J. C., Gonzales, P., Roth, S., Weitman, S., and Wood, K. W. (2004) Antitumor activity of a kinesin inhibitor. *Cancer Res. 64*, 3276–3280.
8. Mayer, T. U., Kapoor, T. M., Haggarty, S. J., King, R. W., Schreiber, S. L., and Mitchison, T. J. (1999) Small molecule inhibitor of mitotic spindle bipolarity identified in a phenotype-based screen. *Science 286*, 971–974.
9. Cox, C. D., Torrent, M., Breslin, M. J., Mariano, B. J., Whitman, D. B., Coleman, P. J., Buser, C. A., Walsh, E. S., Hamilton, K., Schaber, M., Lobell, R. B., Tao, W., South, V. J., Kohl, N. E., Yan, Y., Kuo, L. C., Prueksaritanont, T., Slaughter, D. E., Li, C., Mahan, E., Lu, B., and Hartman, G. D. (2006) Kinesin spindle protein (KSP) inhibitors. Part 4: Structure-based design of 5-alkylamino-3,5-diaryl-4,5-dihydropyrazoles as potent and water soluble inhibitors of the mitotic kinesin KSP. *Bioorg. Med. Chem. Lett. 16*, 3175–3179.
10. Kim, K. S., Lu, S., Cornelius, L. A., Lombardo, L. J., Borzilleri, R. M., Schroeder, G. M., Sheng, C., Rovnyak, G., Crews, D., Schmidt, R. J., Williams, D. K., Bhide, R. S., Traeger, S. C., McConnell, P. A., Mueller, L., Sheriff, S., Newitt, J. A., Pudzianowski, A., Yang, Z., Wild, R., Lee, F. Y., Batorsky, R., Ryder, J. S., Ortega-Nanos, M., Shen, H., Gottardis, M., and Roussell, D. L. (2006) Synthesis and SAR of pyrrolotriazine-4-one based Eg5 inhibitors. *Bioorg. Med. Chem. Lett. 16*, 3937–3942.
11. Cox, C. D., Coleman, P. J., Breslin, M. J., Whitman, D. B., Garbaccio, R. M., Fraley, M. E., Buser, C. A., Walsh, E. S., Schaber, M. D., Lobell, R. B., Tao, W., Davide, J. P., Diehl, R. E., Abrams, M. T., South, V. J., Huber, H. E., Torrent, M., Prueksaritanont, T., Li, C., Slaughter, D. E., Mahan, E., Fernandez-Metzler, C., Yan, Y., Kuo, L. C., Kohl, N. E., and Hartman, G. D. (2008) Kinesin spindle protein (KSP) inhibitors. 9. Discovery of (2S)-4-(2,5-difluorophenyl)-N-[(3R,4S)-3-fluoro-1-methylpiperidin-4-yl]-2-(hydroxymethyl)-N-methyl-2-phenyl-2,5-dihydro-1H-pyrrole-1-carboxamide (MK-0731) for the treatment of taxane-refractory cancer. *J. Med. Chem. 51*, 4239–4252.
12. DeBonis, S., Skoufias, D. A., Indorato, R.-L., Liger, F., Marquet, B., Laggner, C., Benoit, J., and Kozielski, F. (2008) Structure−activity relationship of S-trityl-L-cysteine analogues as inhibitors of the human mitotic kinesin Eg5. *J. Med. Chem. 51*, 1115–1125.
13. Parrish, C. A., Adams, N. A., Auger, K. R., Burgess, J. L., Carson, J. D., Chaudhari, A. M., Copeland, R. A., Diamond, M. A., Donatelli, C. A., Duffy, K. J., Faucetta, L. F., Finer, J. T., Huffman, W. F., Hugger, E. D., Jackson, J. R., Knight, S. D., Luo, L., Moore, M. L., Newlander, K. A., Ridgers, L. H., Sakowicz, R., Shaw, A. N., Sung, C.-m. M., Sutton, D., Wood, K. W., Zhang, S.-Y., Zimmerman, M. N., and Dhanak, D. (2007) Novel ATP-competitive kinesin spindle protein inhibitors. *J. Med. Chem. 50*, 4939–4952.
14. Luo, L., Parrish, C. A., Neysa, N., McNulty, D. E., Chaudhari, A. M., Carson, J. D., Sudakin, V., Shaw, A. N., Lehr, R., Zhao, H., Sweitzer, S., Lad, L., Wood, K. W., Sakowicz, R., Annan, R. S., Huang, P. S., Jackson, J. R., Dhanak, D., Copeland, R. A., and Auger, K. R. (2007) ATP-competitive inhibitors of the mitotic kinesin KSP that function via an allosteric mechanism. *Nat. Chem. Biol. 3*, 722–726.
15. Zhang, B., Liu, J.-F., Xu, Y., and Ng, S.-C. (2008) Crystal structure of HsEg5 in complex with clinical candidate CK0238273 provides insight into inhibitory mechanism, potency and specificity. *Biochem. Biophys. Res. Commun. 372*, 565–570.
16. Annis, D. A., Athanasopoulos, J., Curran, P. J., Felsch, J. S., Kalghatgi, K., Lee, W. H., Nash, H. M., Orminati, J.-P. A., Rosner, K. E., Shipps, G. W., Jr., Thaddupathy, G. R. A., Tyler, A. N., Vilenchik, L., Wagner, C. R., and Wintner, E. A. (2004) An affinity selection-mass spectrometry method for the identification of small molecule ligands for self-encoded combinatorial libraries: Discovery of a novel antagonist of *E. coli* dihydrofolate reductase. *Int. J. Mass Spectrom. 238*, 77–83.
17. Annis, D. A., Nickbarg, E., Yang, X., Ziebell, M. R., and Whitehurst, C. E. (2007) Affinity selection-mass spectrometry screening techniques for small molecule discovery. *Curr. Opin. Chem. Biol. 11*, 518–526.
18. Jackson, J. R., Auger, K. R., Gilmartin, A., Wai, E. K., Luo, L., Concha, N., Parrish, C. A., Sutton, D., Diamond, M. A., Giardiniere, M., Zhang, S.-Y., Huang, P. S., Wood, K. W., Belmont, L., Lee, Y., Bergnes, G., Anderson, R., Brejc, K., and Sakowicz, R. (2005) A resistance mechanism for the KSP inhibitor ispinesib implicates point mutations in the compound binding site, in *Proceedings of the AACR-NCI-EORTC Molecular Targets and Cancer Therapeutics Meeting* (AACR, Philadephia, 2005), Philadelphia, PA.
19. Lahue, B. R., Ma, Y., Shipps, G. W., Jr., Seghezzi, W., and Herbst, R. (2009) Substituted benzimidazoles: A novel chemotype for small molecule hKSP inhibitors. *Bioorg. Med. Chem. Lett. 19*, 3405–3409.
20. Sheth, P. R., Basso, A., Duca, J. S., Lesburg, C. A., Ogas, P., Gray, K., Nale, L., Mannarino, A. F., Prongay, A. J., and Le, H. V. (2009) Thermodynamics of nucleotide and inhibitor binding to wild-type and ispinesib-resistant forms of human KSP. *Biochemistry 48*, 11045–11055.
21. Kayne, F. J. (1973) The Enzymes, Vol. 8, Academic Press, New York.
22. Waldron, T. T., and Murphy, K. P. (2003) Stabilization of proteins by ligand binding: Application to drug screening and determination of unfolding energetics. *Biochemistry 42*, 5058–5064.
23. Brandts, J. F., and Lin, L. N. (1990) Study of strong ultratight protein interactions using differential scanning calorimetry. *Biochemistry 29*, 6927–6940.
24. Mayhood, T. W., and Windsor, W. T. (2005) Ligand binding affinity determined by temperature-dependent circular dichroism: Cyclin-dependent kinase 2 inhibitors. *Anal. Biochem. 345*, 187–197.
25. Lad, L., Luo, L., Carson, J. D., Wood, K. W., Hartman, J. J., Copeland, R. A., and Sakowicz, R. (2008) Mechanism of inhibition of human KSP by ispinesib. *Biochemistry 47*, 3576–3585.
26. Luo, L., Carson, J. D., Dhanak, D., Jackson, J. R., Huang, P. S., Lee, Y., Sakowicz, R., and Copeland, R. A. (2004) Mechanism of inhibition of human KSP by monastrol: Insights from kinetic analysis and the effect of ion strength on KSP inhibition. *Biochemistry 43*, 15258–15266.
27. Knight, S. D., and Parrish, C. A. (2008) Recent progress in the identification and clinical evaluation of inhibitors of the mitotic kinesin KSP. *Curr. Top. Med. Chem. 8*, 888–904.
28. Rickert, K. W., Schaber, M., Torrent, M., Neilson, L. A., Tasber, E. S., Garbaccio, R., Coleman, P. J., Harvey, D., Zhang, Y., Yang, Y., Marshall, G., Lee, L., Walsh, E. S., Hamilton, K., and Buser, C. A. (2008) Discovery and biochemical characterization of selective ATP competitive inhibitors of the human mitotic kinesin KSP. *Arch. Biochem. Biophys. 469*, 220–231.
29. Pantoliano, M. L., Petrella, E. C., Kwasnoski, J. D., Lobanov, V. S., Myslik, J., Graf, E., Carver, T., Asel, E., Springer, B. A., Lane, P., and Salemme, F. R. (2001) High-density miniaturized thermal shift assays as a general strategy for drug discovery. *J. Biomol. Screen. 6*, 429–440.
30. Berenbaum, M. C. (1989) What is synergy? *Pharmacol. Rev. 41*, 93–141.
31. Tallerida, R. J. (2000) Drug Synergism and Dose-Effect Data Analysis, Chapman & Hall/CRC, Boca Raton, FL.